Electronic Supplementary Material (ESI) for Physical Chemistry Chemical Physics.
This journal is © the Owner Societies 2017

Electronic Supplementary Information

Controlled Solvent Vapor Annealing of a High χ Block Copolymer Thin Film

Ross Lundy*^,1,2^, Shauna P. Flynn[3], Cian Cummins[4], Susan M. Kelleher[3], Maurice N. Collins[2], Eric Dalton[2], Stephen Daniels[3], Michael A. Morris[4] and Ryan Enright*^,1^

[1]Thermal Management Research Group, Efficient Energy Transfer (ηET) Dept., Bell Labs Ireland, Nokia, Blanchardstown Business & Technology Park, Snugborough Rd. Dublin 15, Ireland
[2]Stokes Laboratories, University of Limerick, Co. Limerick, Ireland
[3]National Centre for Plasma Science and Technology, Dublin City University, Glasnevin, Dublin 9, Ireland.
[4]AMBER @ CRANN, Trinity College Dublin, Dublin, Ireland
*** Corresponding author: ross.lundy2@gmail.com, ryan.enright@nokia.com**

Section S1 - Flory-Huggins interaction parameter estimation

In order to estimate the Flory-Huggins interaction parameter where one was not readily available, we followed the Hansen solubility method[1]. In the Hansen approach the Flory-Huggins interaction parameter is given by

$$\chi_{AB} = \frac{V_m}{4RT}\left[4\left(\delta_{d,A} - \delta_{d,B}\right)^2 + \left(\delta_{p,A} - \delta_{p,B}\right)^2 + \left(\delta_{h,A} - \delta_{h,B}\right)^2\right], \qquad \textbf{Eq. S1}$$

where *R* is the universal gas constant and *T* is absolute temperature. The material specific solubility parameters for non-specific dispersive (δ_d), specific polar (δ_p) and specific hydrogen bonding (δ_h) interactions can be found from tabulated sources or estimated from group methods[1,2]. For solvent-polymer interactions, we use the molecular volume of the solvent in our calculations, $V_m = V_S$. For polymer-polymer interactions we use the geometric mean of the molecular volumes for the respective monomers, $V_m = \bar{V}_{AB} = [(\nu_A M_A)(\nu_B M_B)]^{1/2}$, where ν and *M* are the monomer specific volume and molecular weight, respectively. ***Table S1*** tabulates the solubility parameters used to estimate the χ values given in ***Table S2*** and used in our subsequent calculations. Note that the estimated value of $\chi_{PS\text{-}P4VP} = 0.524$ compares well to the value of $\chi_{PS\text{-}P4VP} = 0.559$ calculated from the regression expression given by Zha *et al* [3]

Table S1 System molecular volumes and Hansen solubility parameters.

Species	V_m (μm^3/mol)	δ_d (MPa$^{0.5}$)	δ_p (MPa$^{0.5}$)	δ_h (MPa$^{0.5}$)
4-vinylpyradine	108	18.1	7.2	6.8
Styrene	115	18.6	1.0	4.1
Tetrahydrofuran	81.7	16.8	5.7	8
Ethylene glycol	57.6	17	11	26

Table S2 **System Flory-Huggins interaction parameters estimated using Eq. S1 at $T = 294$ K.**

Combination	PS/P4VP	PS/THF	P4VP/THF	EG/THF	P4VP/EG	PS/EG
χ	0.524	0.414	0.086	2.44	2.26	3.53

Section S2 - As spun PS-b-P4VP film

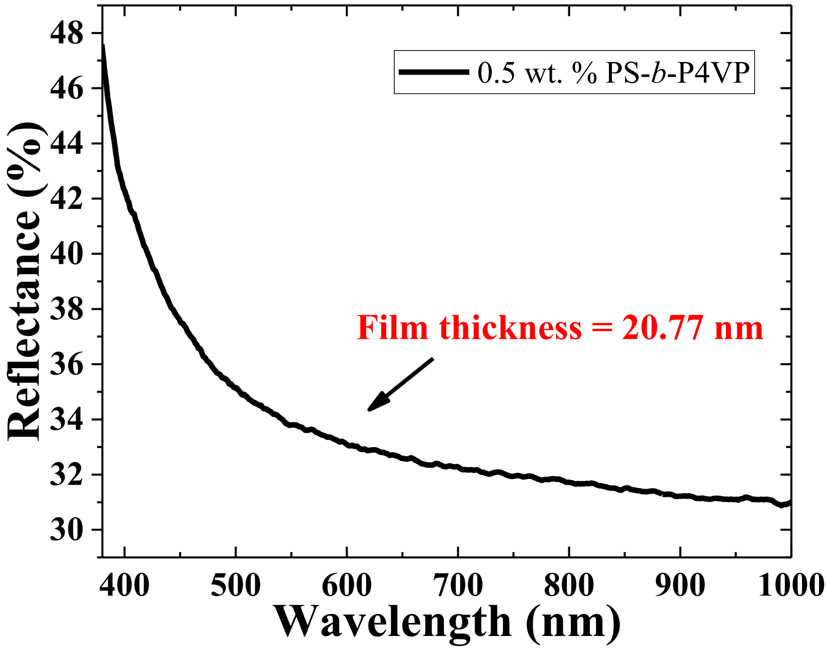

Figure S1 Film thickness measured using ex-situ spectral reflectometry for an annealed 0.5 wt. % PS-b-P4VP. The model fit indicates a film thickness of $L = 20.77$ nm. Goodness of fit = 0.998 with model.

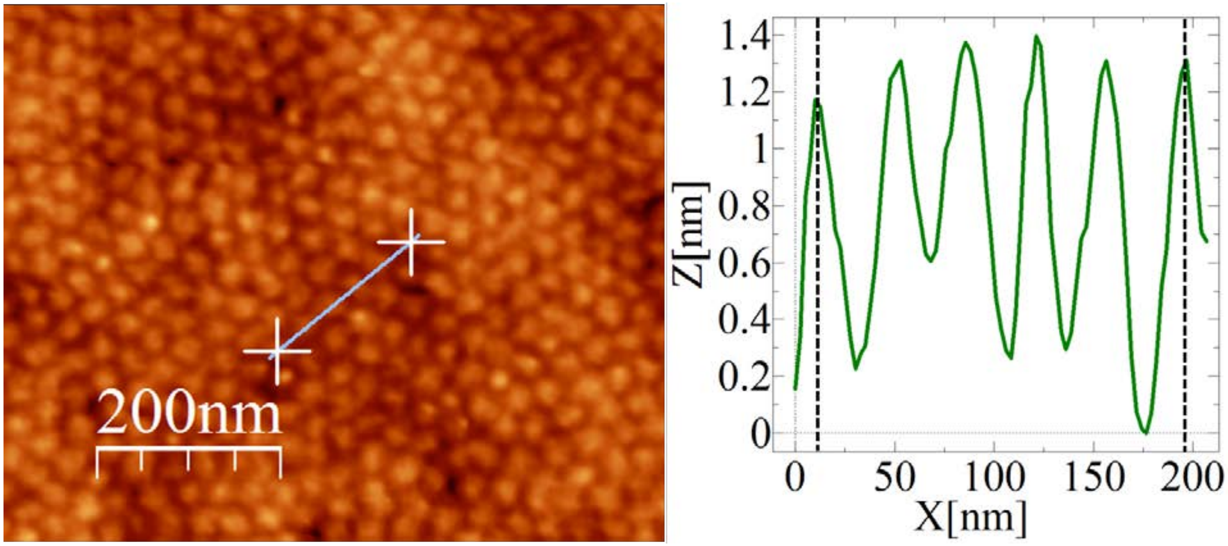

Figure S2 The AFM height image shows an as-spun un-annealed 0.5 wt. % PS-b-P4VP film. The as-cast film shows micelle like features. The line profile measured across 6 features gives a center-to-center spacing of ~ 36 nm.

Section S3 - dSVA System Design Details

Chamber design

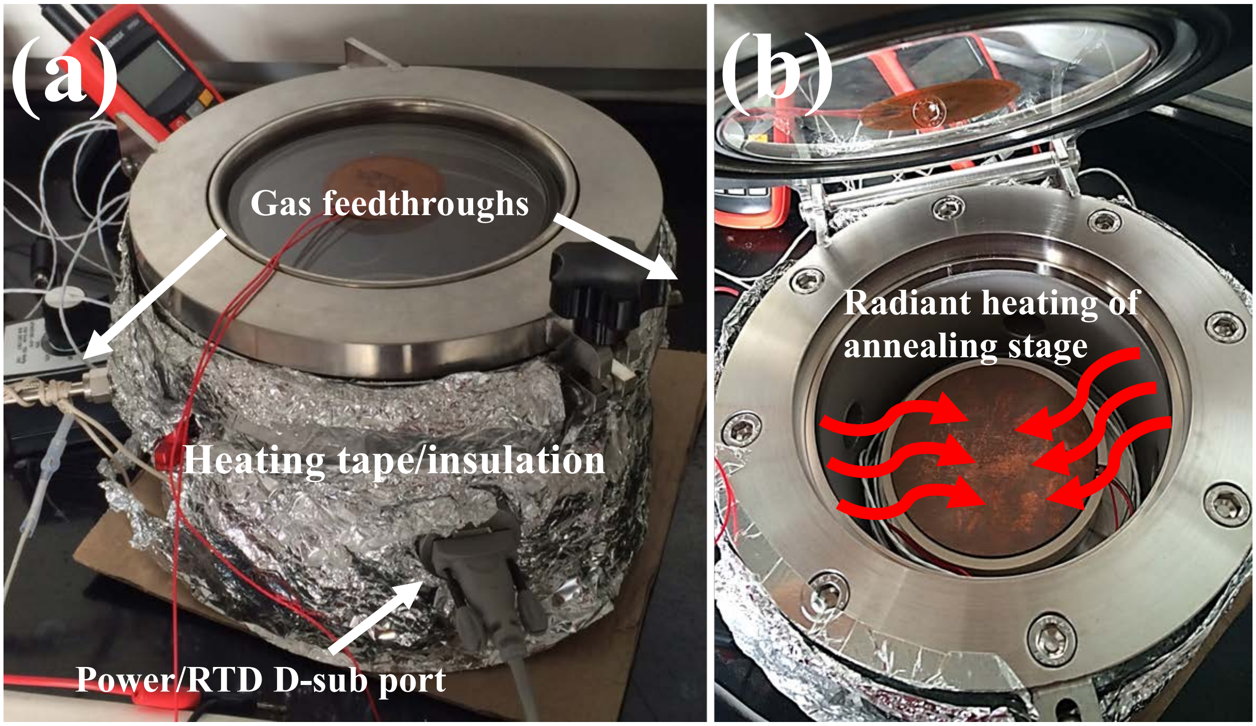

Figure S3 The chamber was fabricated by combining a stainless steel ISO straight connector with an access door and viewport (top) and blank rotatable flange (bottom). 4 feedthrough ports were added at 90 ° interval around the middle of the chamber (gas in and out, D-sub connector and a blank). All steel pipes connecting the bubbler to chamber are heated using rope heaters.

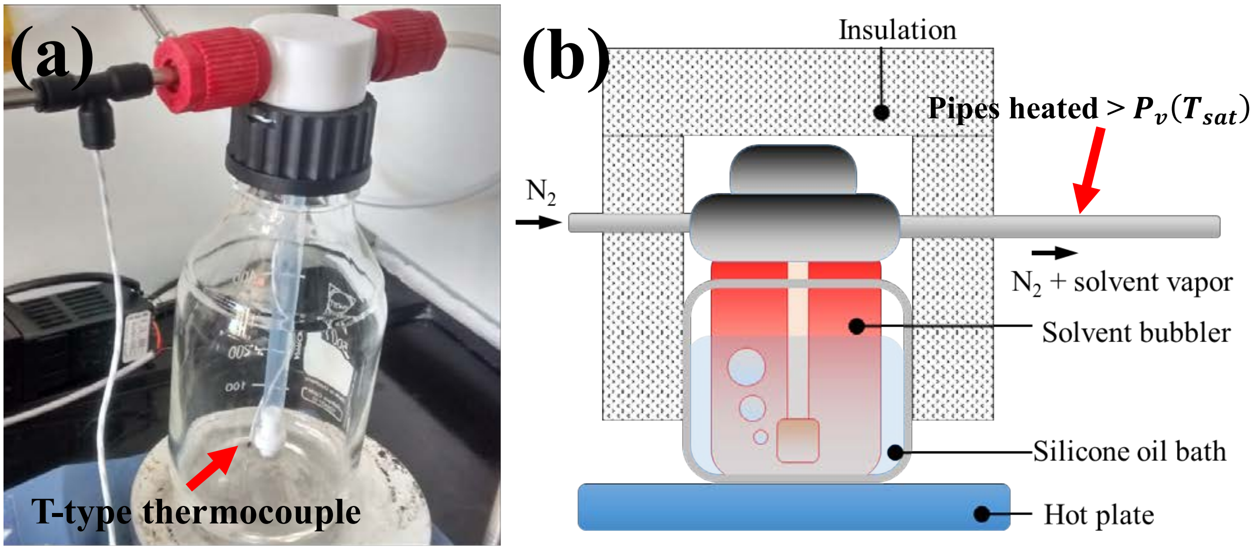

Figure S4 Bubbler with in-situ thermocouple probe is immersed in silicone oil and insulated. The pipes were heated using rope heaters to prevent a drop in vapor pressure as a result of condensation within the pipes.

Annealing stage design

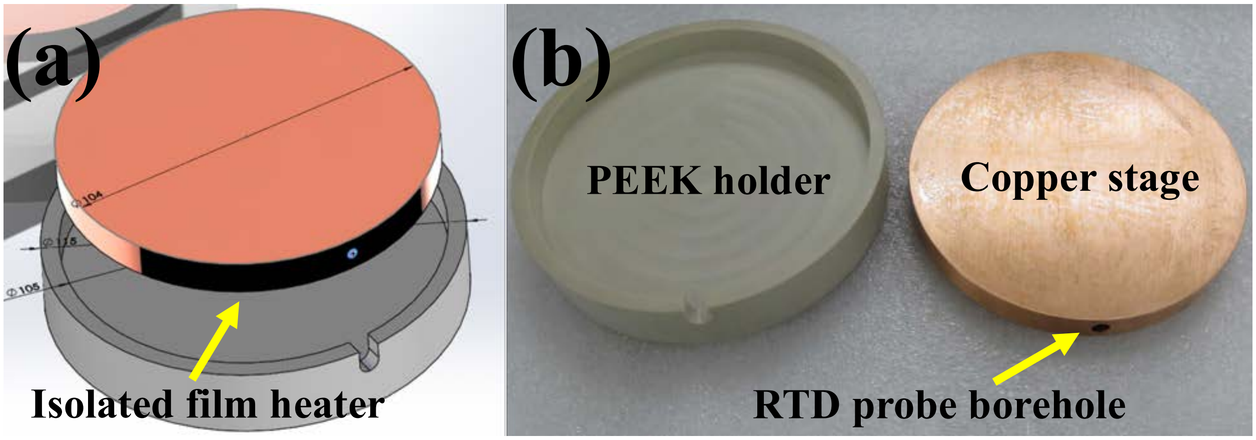

Figure S5 (a) 3D assembly of the annealing stage created using SolidWorks[4]. A 110V flexible polyimide film heater is placed between the copper stage and PEEK holder using pressure sensitive adhesive. This setup ensures that the heating element is isolated from the solvents used during annealing. The assembly was designed to account for thermal expansion of materials and allow for accurate placement of an RTD probe for temperature feedback. Polyether ether ketone (PEEK) was chosen as the material for the holder (shown in (b)) due to its rigid structure, favorable insulating properties and very high chemical resistance to most solvents. Oxygen free Copper (OFC) was used for the heating stage for its high thermal conductivity. A (Ø2.5 mm) borehole was fabricated on the side of the OFC plate for optimal RTD probe placement. For a more detailed design see computer aided design (CAD) drawings in Figure S4 and Figure S5. The proportional integral derivative (PID) controller setup (Figure S6) allows for precise temperature control of the copper annealing stage to within ± 0.15 °C (Class A RTD probe tolerance @ 0 °C).

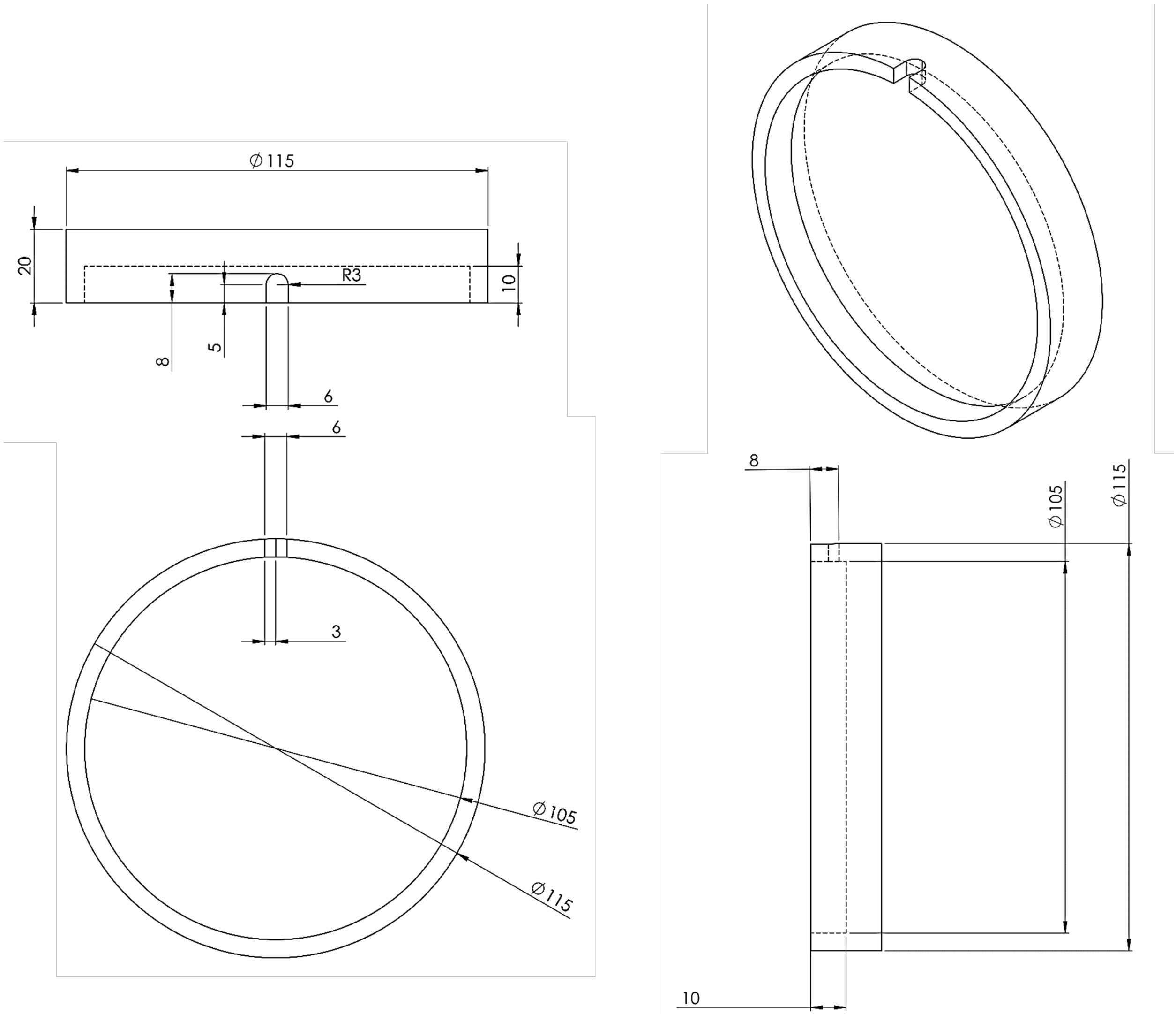

Figure S6 Orthographic and isometric CAD drawings [4] of PEEK holder for copper plate.

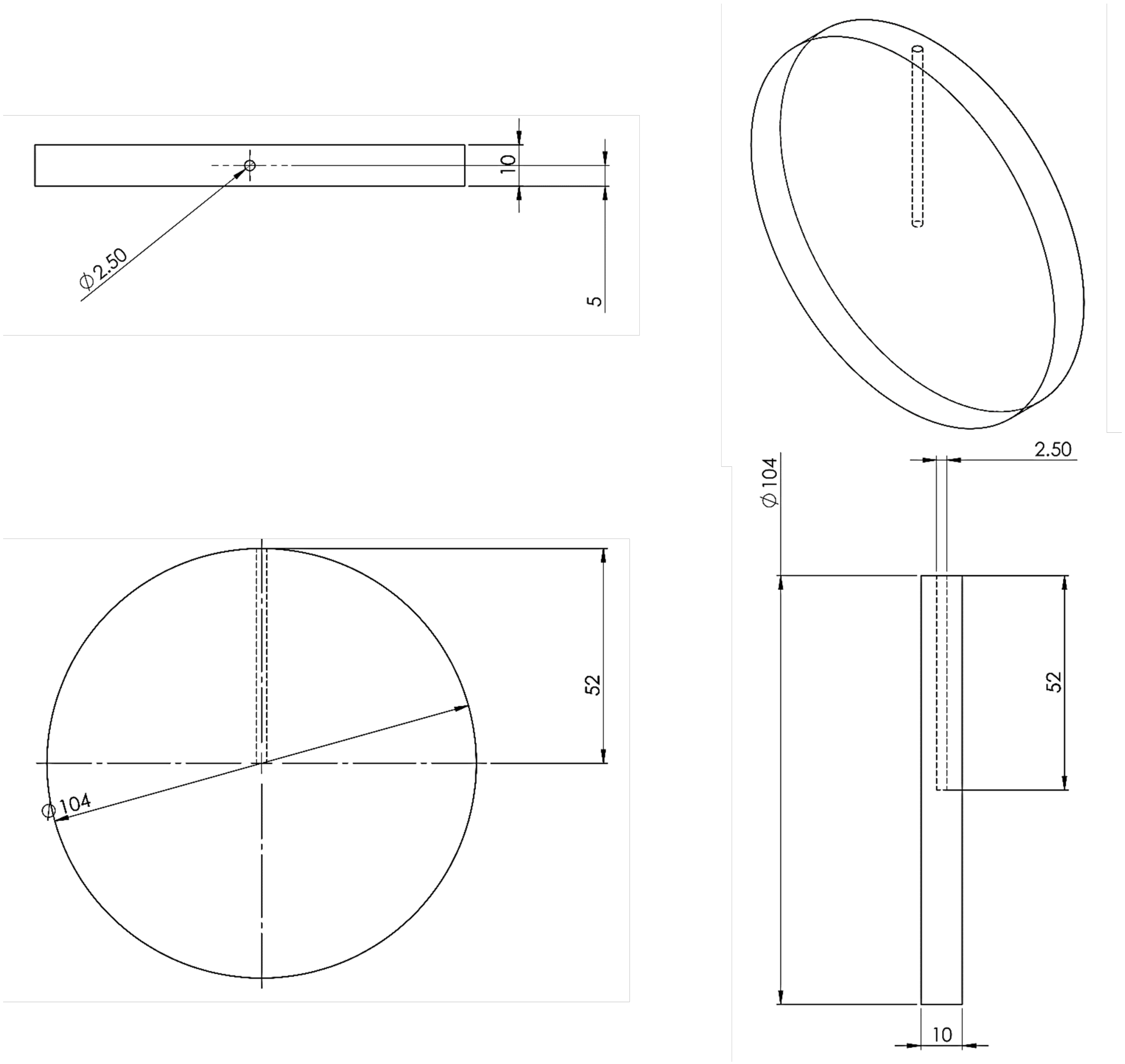

Figure S7 Orthographic and isometric CAD drawings[4] of copper plate for annealing stage.

Stage temperature control wiring

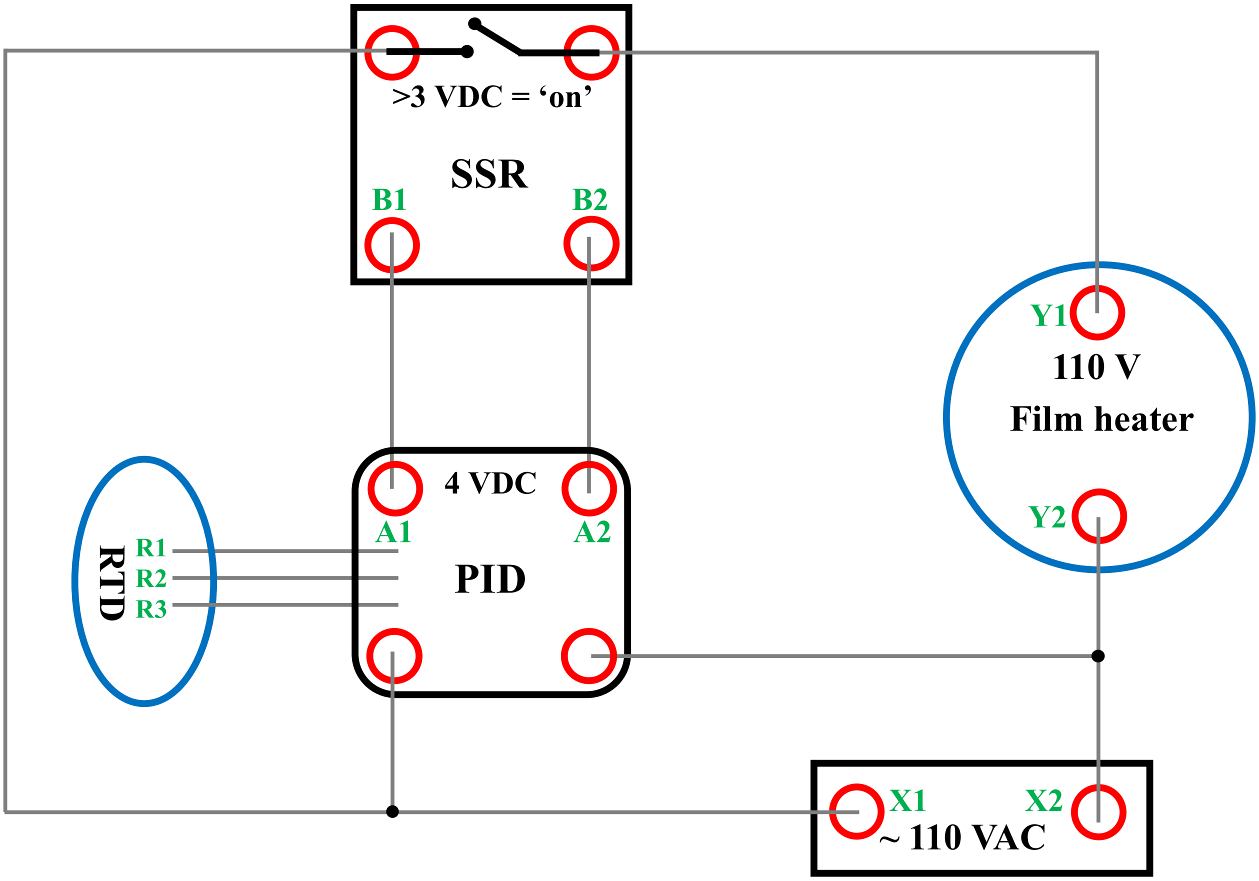

Figure S8 Circuit diagram of the temperature control setup used for the heating stage. A 220 VAC to 110 VAC step down transformer is used for supplying power to the PID controller and the film heater within the annealing stage. The platinum tip in the RTD probe is rated as 100 Ω at 0 °C and increases with temperature. The PID controller applies a voltage across wires $R1 + R2$ of the RTD probe and by measuring the electrical resistance across the platinum tip (R_{Pt}), temperature can be determined. Since there is a resistance associated with the wires the total resistance measured is $R_{tot} = R_{Pt} + R1 + R2$, which would lead to an uncertainty in the measured temperature. A 3-wire RTD setup is used to account for this unwanted resistance. The PID measures the lead resistance across wires $R2 + R3$ (equivalent to resistance across $R1 + R2$) and subtracts from the total measured resistance leaving just the resistance of: $R_{Pt} = R_{tot} - (R2 + R3)$. If measured temperature < set point temperature the PID passes a 4 VDC control signal (A1/A2) to the control terminals (B1/B2) on the solid state relay (SSR). A sensor in the SSR responds to a control signal > 3 VDC, activating the electronic switch in the SSR to an 'on' state allowing current to flow between the 110 VAC power supply (X1/X2) and the Film heater (Y1/Y2).

Section S4 - Additional AFM and FESEM data

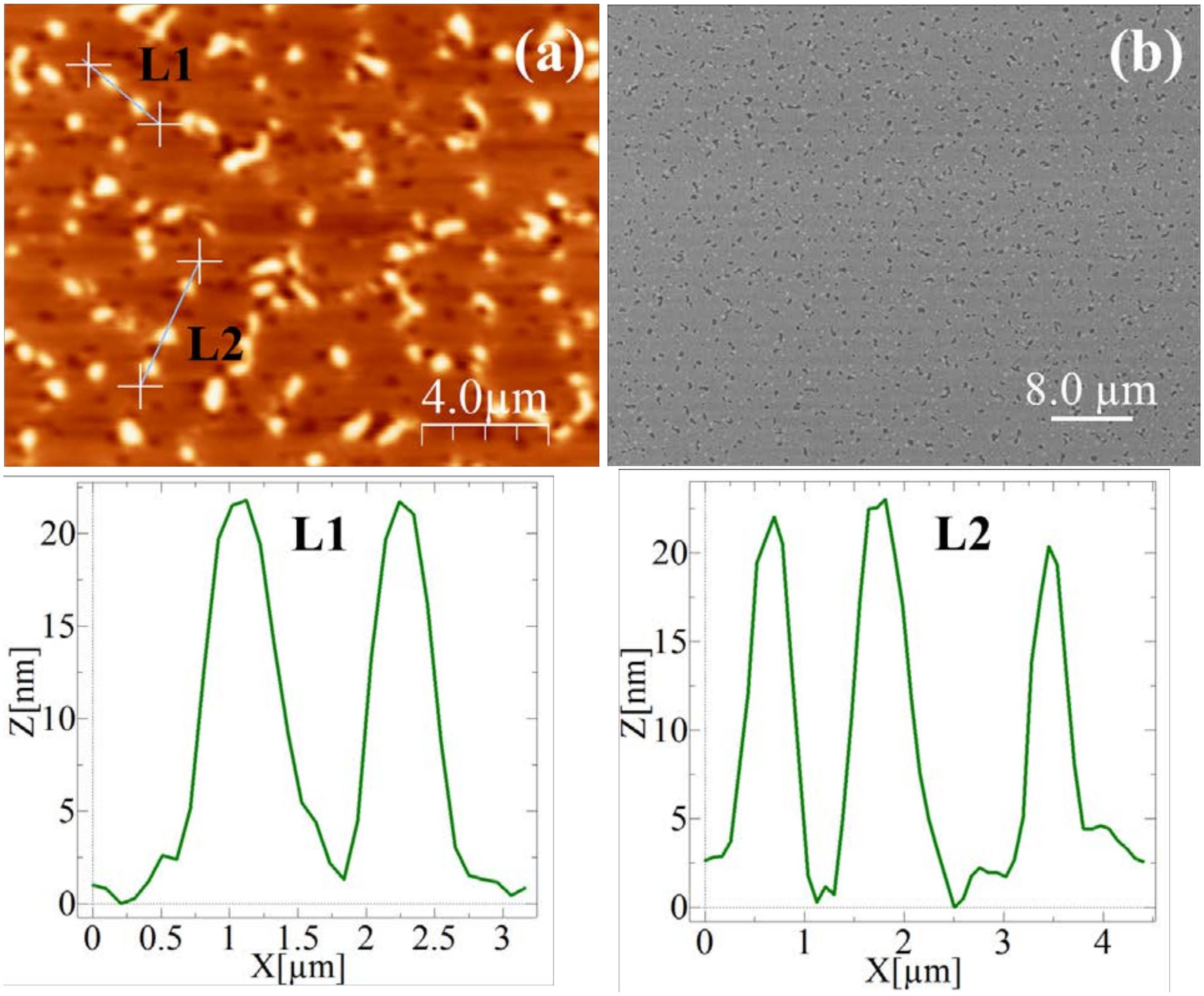

Figure S9 The AFM image in (a) and FESEM image (b) are of an as annealed 0.5 wt. % PS-*b*-P4VP using static solvent annealing in THF for 4 hours at 50 °C. Small dark circles were observed in (a) but were too small to accurately characterize. Islands were observed and can also be seen in the FESEM image (b) at a similar length scale. The graphs L1 and L2 verify these undulations which have a height of ~20 nm. Higher resolution images in Figure 1 (d), (e) (manuscript) and Figure S10 show the islands in more detail and also verify and characterize the dewetted unpatterned regions

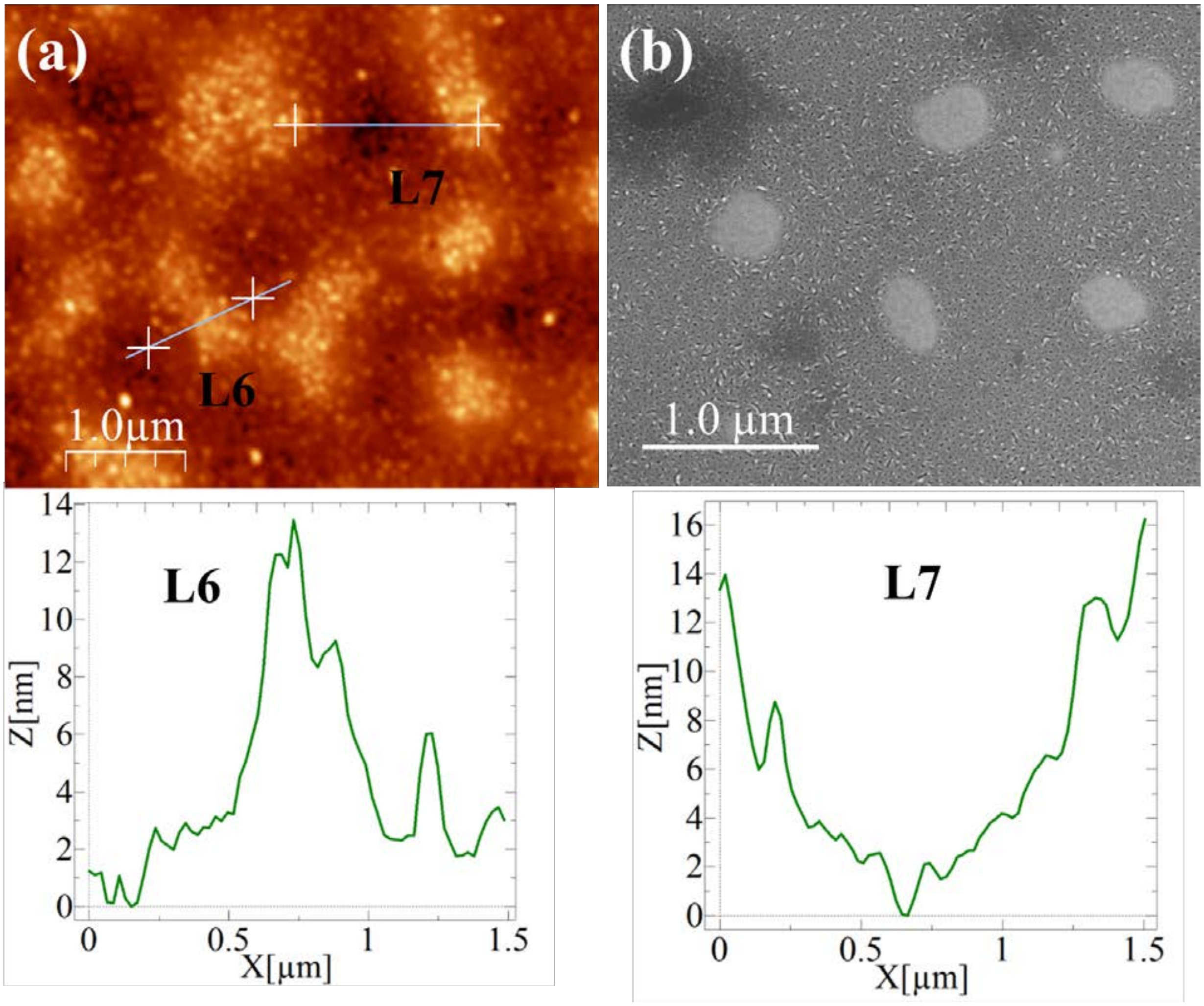

Figure S10 More detail is seen at higher resolutions in (a) with the height profiles of the dewetted regions and islands measured in L6 and L7. Surface reconstruction using ethanol was performed on the sample and imaged in (b) using FESEM to show any unpatterned regions. The dewetted light colored holes show no pattern as expected. The dark island regions are still patterned.

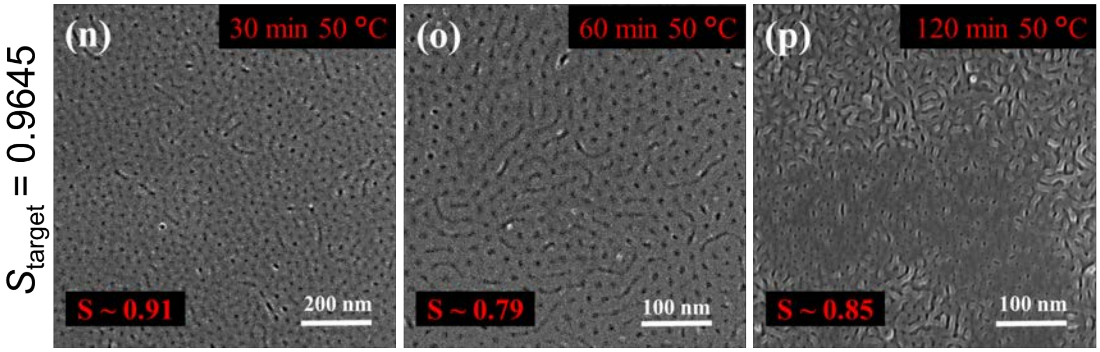

Figure S11 FESEM micrographs of reconstructed BCP films using dSVA at 50 °C for various times. The annealing time and solvent bubbler temperatures are indicated in the top right inset of each image. The targeted annealing supersaturation based on controlling T_{sub} to T_{sat} + 1 K is given to the left of each row. The actual supersaturation level achieved for each anneal are given in the bottom left inset of each image.

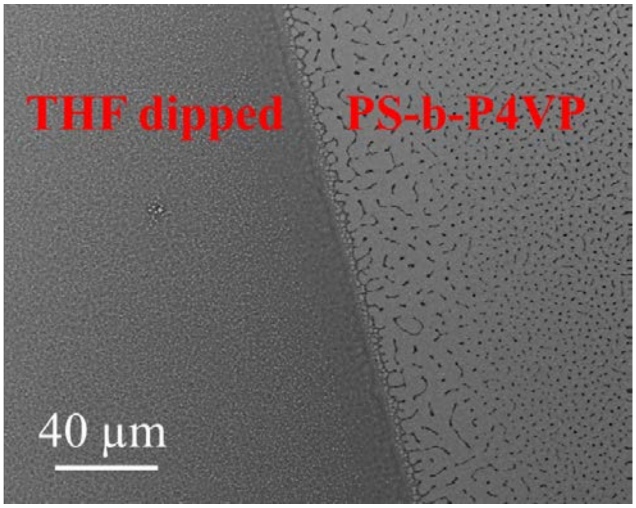

Figure S12 FESEM micrograph of an as annealed 0.5 wt. % PS-*b*-P4VP using static solvent annealing in THF for 4 hours at 50 °C. The substrate was subsequently partially dipped in a pure THF solution for ~ 1 second resulting in dissolution of the polymer film as shown on the left-hand side of the image.

Section S5 - Supersaturation uncertainty calculation

The solvent vapor pressure will drop during annealing if nucleation occurs within the chamber. To prevent this the outside of the chamber is heated by wrapping and insulating resistive heating tape around the chamber as shown in Figure S3 (a). Ideally the chamber should be heated to the same temperature as the annealing stage but precise temperature control of the internal chamber walls is not possible due to temperature gradients around the thick stainless steel chamber, thus the whole chamber is heated above the annealing stage and bubbler temperature by ~ 10 °C. The negative effect of this is that the annealing stage temperature will increase slightly due to radiant heating over the course of an anneal shown in Figure S3 (b) leading to an increase in $P_v(T_{sub})$. This effect results in a lower than desired supersaturation $S = P_v(T_{sat})/P_v(T_{sub})$. Since an N_2 flowrate of 120 ml/min is used, it takes ~ 15 minutes for $P_v(T_{sat})$ to reach its maximum pressure within the chamber (internal chamber volume 1.9 L). Therefore, calculating S is more accurately based on the temperatures at the end of the anneal.

As an example, anneal (f) had temperatures of T_{sat} = 30.4 °C and T_{sub} = 31.3 °C for the bubbler and annealing stage respectively at the end of the anneal. The Antoine equation ($P = 10^{A-\frac{B}{C+T}}$) where P is pressure in mmHg, T is temperature in °C and the parameters $A = 6.99515$, $B = 1202.29$ and $C = 226.254$ were taken from DDBST[5] and used to calculate THF partial pressures of $P_v(T_{sub}) = 28.3103\ kPa$ and $P_v(T_{sat}) = 26.8079\ kPa$, giving a value for $S = 0.947$. The uncertainty ($\omega_S = 0.041$) of S was calculated by considering the propagation of uncertainties

$$\omega_S = \sqrt{\left(\frac{\partial S}{\partial T_{sat}} . \omega_{T_{sat}}\right)^2 + \left(\frac{\partial S}{\partial T_{sub}} . \omega_{T_{sub}}\right)^2},$$

where $\omega_{T_{sat}}$ = 0.5 °C and $\omega_{T_{sub}}$ = 0.15 °C are the uncertainties of the T-type thermocouple and RTD probe temperature measurements, respectively. Table 1 shows the S values for each of the annealing experiments.

Table S3 – Calculated supersaturation S values for the anneals in Figure 3 of the manuscript.

Anneal	S (15 min)	S (30 min)	S (60 min)	S (120 min)
21 °C (a-d)	0.852±0.042	0.913±0.038	0.794±0.045	0.913±0.038
30 °C (e-h)	0.939±0.041	0.947±0.041	0.901±0.045	0.829±0.052
40 °C (i-l)	0.943±0.047	0.943±0.047	0.841±0.06	0.81±0.065
50 °C (m-p)	0.92±0.057	0.909±0.057	0.792±0.083	0.851±0.07

Section S6 - Phase segregation time-scale estimation

In order to estimate the characteristic diffusivity governing the phase segregation of the PS-b-P4VP film, we follow the review of Yokoyama [6]. The translational diffusivity of the polymer based on Rouse's model (hydrodynamic interactions neglected) is given by

$$D_{tr} = \frac{k_b T}{N\xi}, \qquad \textbf{Eq. S2}$$

where k_b (= 1.38065×10^{-23} J/K) is Boltzmann's constant, N is the degree of polymerization and $\xi(\phi_p, T)$ is the solvent concentration and temperature dependent monomer friction coefficient. Here we assume that ξ is the same for both the PS and P4VP blocks and estimate its value from the experimental diffusion data of methyl red in PS/THF solutions[7]. **Figure S13** plots the extracted monomer friction coefficient over the range of our experimental conditions.

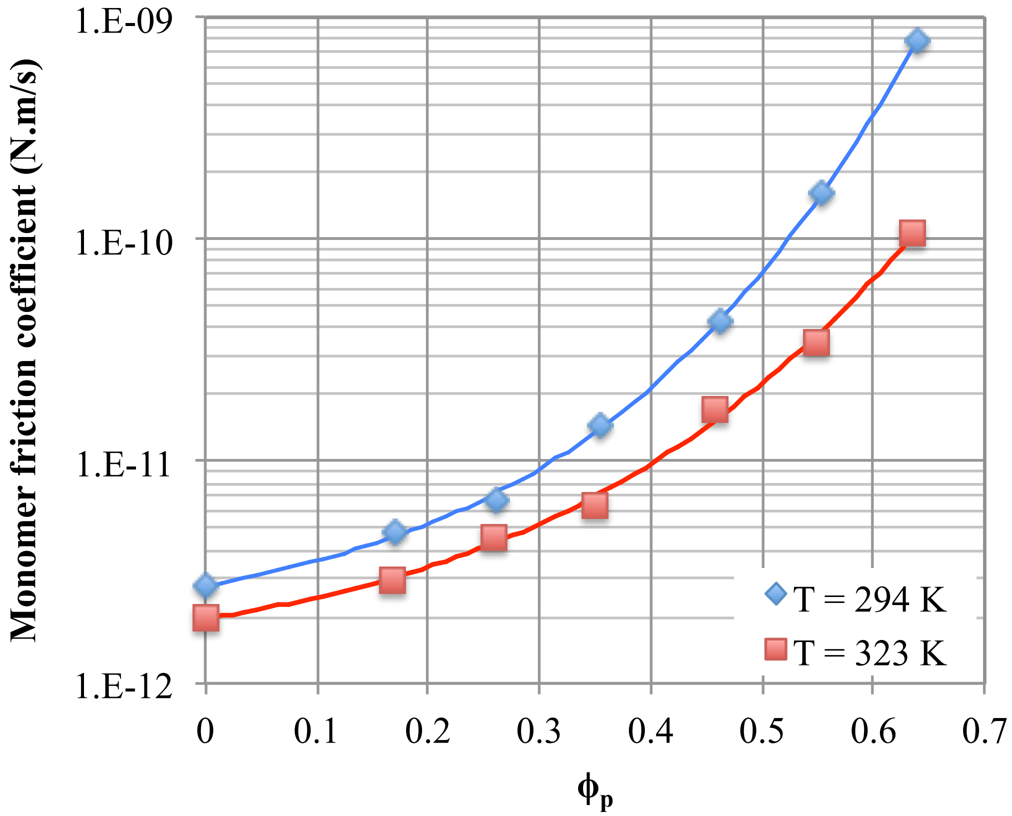

Figure S13 PS monomer friction coefficient in THF. Points were extracted from the data of Landry *et al.*[7] At each concentration by extrapolating to the indicated temperature using an Arrhenius fit. The lines represent a fit to the data points using a logarithmic scaling with a 3rd order polynomial fit for the exponent. Both fits demonstrate an $R^2 > 0.999$.

In the cylinder forming system diffusion is anisotropic with relatively fast interface diffusion taking place along the axis of the cylinders with the comparatively slower hopping diffusion associated with block retraction taking place normal to the cylinder axis. This activated (hopping) diffusivity is given by

$$D_a = D_{tr} \exp\left(-\alpha\left[\chi_{eff} N_A - (\chi N_A)_{ODT}\right]\right), \qquad \textbf{Eq. S3}$$

where $\alpha \approx 1.2$ is an experimentally found constant[6], χ_{eff} is the solvent concentration dependent interaction parameter between the two blocks, N_A is the minority block (P4VP) degree of polymerization and $(\chi N_A)_{ODT}$ identifies the order-disorder transition. Based on the classical phase map[8], for $f(\phi_p) = f_{4VP} = 0.28$ we expect a phase segregated pattern of hexagonal cylinders and $\chi N_{\mathrm{ODT}} \sim 15$, corresponding to $\chi N_A \sim 4.2$ where $N_A = N_{4VP} = 90$.

The effective interaction parameter governing local block interactions is expected to follow the dilution approximation[9]

$$\chi_{eff} = \phi_p \chi_{AB}, \qquad \textbf{Eq. S4}$$

A smoothly varying expression for the diffusivity around the ODT is then defined as

$$D = D_{tr}\left(\frac{1}{1 + D_{tr}/D_a}\right). \qquad \textbf{Eq. S5}$$

The characteristic time-scale for phase segregation is then defined as

$$t_{tr} = \frac{l^2}{2D}, \qquad \textbf{Eq. S6}$$

where l is the characteristic length scale for the phase-segregated BCP pattern, which, based on our experimental observations, we assign a value of 26 nm.

In order to link the film polymer concentration to the experimentally-controlled solvent vapor saturation $S = P_v(T_{sat})/P_v(T_{sub})$, where $P_v(T_{sat})$ and $P_v(T_{sub})$ are the solvent vapor pressure at the vapor saturation temperature and substrate temperature, respectively, we use the Flory-Huggins equation [10]

$$\ln S = \chi_{SAB}\phi_p^2 + \ln(1 - \phi_p) + (1 - N^{-1})\phi_p, \qquad \textbf{Eq. S7}$$

where N is the degree of polymerisation and χ_{SAB} is the interaction parameter between the diblock copolymer and the solvent that is estimated according to the Scott-Flory-Huggins formalism, resulting from a mean-field approach for a binary mixture of a random copolymer and a probe [11]

$$\chi_{SAB} = f_A\chi_{SA} + (1 - f_A)\chi_{SB} - f_A(1 - f_A)\chi_{AB}\left(\frac{V_S}{\bar{V}_{AB}}\right), \qquad \textbf{Eq. S8}$$

where f_A is the block fraction and $V_S/\bar{V}_{AB}$ is the ratio of the solvent molecular volume to the geometric mean of the copolymer molecular volume.

Figure S14 plots the characteristic phase segregation timescale (**Eq. S6**) as a function of solvent supersaturation (**Eq. S7**).

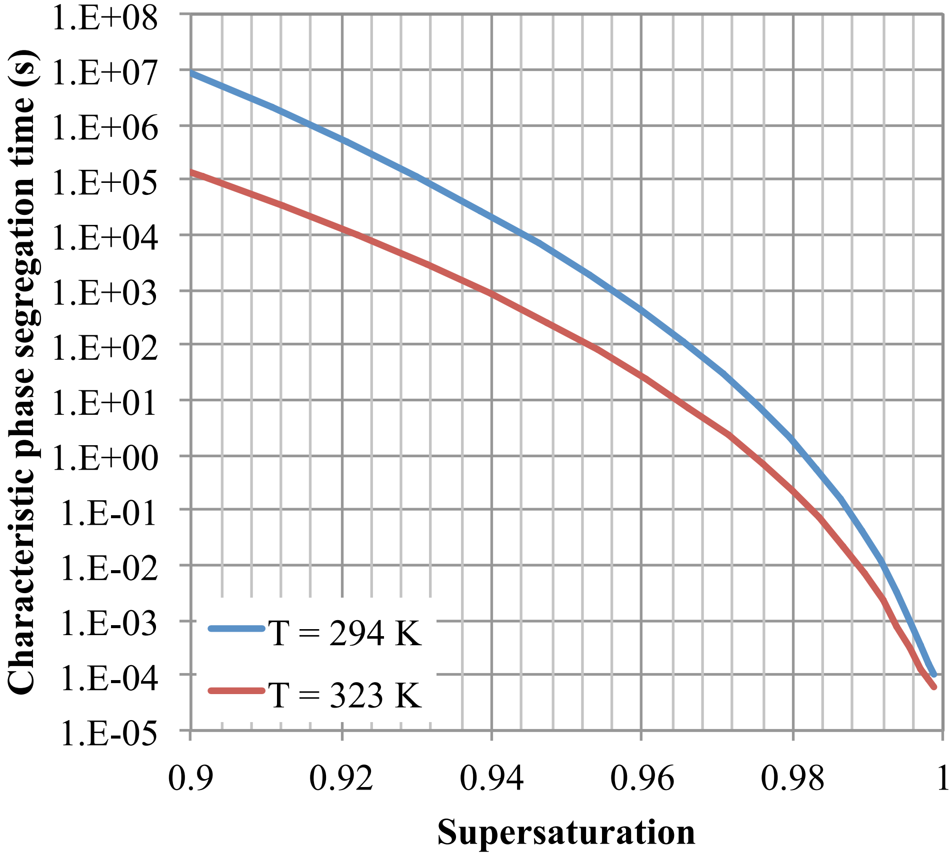

Figure S14 Characteristic phase segregation time as a function of solvent vapor supersaturation for the minimum and maximum annealing temperatures investigated with *l* = 26 nm.

We estimated the ODT based on non-linear scaling. For non-selective good solvents ($\chi_{AS} - \chi_{BS} = 0$), Lodge *et al*. have shown that the dilution approximation breaks down for small ϕ_p resulting in a non-linear dependence on ϕ_p, $\chi_{eff} = \chi_{AB}\phi_p^n$, where the exponent *n* has a theoretical value of ~1.6. Lodge has found experimentally for P(S-b-I) systems that the exponent varies between ~1.3 and 1.6 as N is increased[9]. Assuming $n = 1.3$ for our relatively low N system, we estimate the ODT to occur at $S \approx 0.99$ for the range of annealing temperatures explored.

Section S7 - Energy balance equation

We can perform a simple surface energy balance to estimate the temperature difference between the polymer surface and the RTD embedded in the wafer stage due to heat losses associated with sensible heat transfer into the solvent vapour and radiative heat transfer from the heated walls of the chamber.

The energy balance has the form

$$q''_{cond} - q''_{conv} = q''_{rad}$$

The conductive term is estimated as

$$q''_{cond} = \frac{(T_{RTD} - T_{BCP})}{R'_T}$$

where the series resistivity between the embedded RTD in the copper stage at temperature T_{RTD} and the surface of the BCP thin film exposed to the solvent vapour at temperature T_{BCP} is

$$R'_T = \frac{L_{Cu}}{k_{Cu}} + \frac{L_f}{k_f} + \frac{L_{Si}}{k_{Si}} + \frac{L_{BCP}}{k_{BCP}}$$

that is composed of a copper layer of thickness L_{Cu} and thermal conductivity k_{Cu}. Similar layers are defined for a thin resistive interface between the copper stage and the silicon wafer (L_f, k_{f}), for the silicon wafer (L_{Si}, k_{Si}) and the BCP film (L_{BCP}, k_{BCP}).

The convective term capturing sensible heat lost from the BCP film to the solvent vapor is estimated as

$$q''_{conv} = h(T_{BCP} - T_{sat}) \approx \frac{k_{THF,v}}{l}(T_{BCP} - T_{sat})$$

where we define the heat transfer coefficient as $h = k_{THF,v}/l$, the ratio of the THF solvent vapour thermal conductivity (taken as dry air) and the characteristic boundary layer thickness given by [12]

$$l = D\left[0.664 Re^{1/2} Pr^{1/3}\right]^{-1}.$$

Based on the nominal flow rate through the chamber (Q = 120 mL/min) and the approximate cross sectional area of the chamber ($A = D_c\pi/2 \approx 0.1$ m^2) , we estimate $u = 2 \times 10^{-4}$ m/s, $Re = uD_c/\nu = 1.8$. Considering dry air properties at 50 °C ($Pr = 0.7$, $\nu = 1.7 \times 10^{-5}$ m^2/s), we determine $l \approx 188$ mm. Since this is larger than the gap between the wafer and the chamber lid in our experiments, we conservatively use the physical dimension of the gap (~100 mm) to define l.

Finally, the radiative term capturing heat transfer from the hot chamber walls to the BCP film is estimated by linearizing the Stefan-Boltzmann equation

$$q''_{rad} = \epsilon\sigma(T^4_{wall} - T^4_{BCP}) \approx \epsilon\sigma T^3_m(T_{wall} - T_{BCP})$$

where T_{wall} is the temperature of the chamber walls, ϵ is the surface emissivity and σ ($\approx 5.67 \times 10^{-8}$ W.m^{-2}.K^{-4}) is the Stefan-Boltzmann constant.

Of particular interest is the estimated temperature difference between the RTD embedded in the copper stage and the surface of the BCP thin film exposed to the solvent vapour. Based on the relevant experimental parameters under worst-case conditions (see Table xx), we estimate that $T_{\mathrm{RTD}} - T_{\mathrm{BCP}} = -0.015$ during annealing. Thus, this simple analysis suggests that the BCP/solvent vapour interface may be slightly hotter than the embedded RTD due to radiative heating from the chamber walls, which is consistent with our observation of the stage heating up during the annealing process. If we allow $T_{\mathrm{w}} \rightarrow T_{\mathrm{RTD}}$ to remove the radiative contribution, we find $T_{\mathrm{RTD}} - T_{\mathrm{BCP}} < 1$ mK. We conclude that sensible heat transfer from the BCP film to the solvent vapour is negligible, but better control over $T_{\mathrm{w}} - T_{\mathrm{RTD}}$ is advantageous to ensure $T_{\mathrm{BCP}} \approx T_{\mathrm{RTD}}$.

Table 1 – Parameters used in calculating the energy balance.

k_{BCP}	~0.15 W/m.K[a]
k_{Cu}	~400 W/m.K
k_f	0.1 W/m.K[b]
k_{Si}	~150 W/ m.K
$k_{THF,v}$	0.028 W/m.K[c]
L_{BCP}	~100 nm
L_{Cu}	~1 mm
L_f	10 μm
L_{Si}	400 μm
T_{RTD}	325 K
T_{sat}	323 K
$\boldsymbol{T}_{\mathbf{wall}}$	333 K
ϵ	1

a. Liquid THF value at ~50 °C.
b. Dry contact effective thermal conductivity.
c. Dry air value at ~50 °C.

References.

(1) Hansen, C. M. *Hansen Solubility Parameters: A User's Handbook*; CRC press, 2007.

(2) Starý, Z. Thermodynamics and Morphology and Compatibilization of Polymer Blends. In *Characterization of Polymer Blends*; Wiley-VCH Verlag GmbH & Co. KGaA, 2014; pp 93–132.

(3) Zha, W.; Han, C. D.; Lee, D. H.; Han, S. H.; Kim, J. K.; Kang, J. H.; Park, C. Origin of the Difference in Order–Disorder Transition Temperature between Polystyrene-Block-poly(2-

Vinylpyridine) and Polystyrene-Block-poly(4-Vinylpyridine) Copolymers. *Macromolecules* **2007**, *40* (6), 2109–2119.

(4) SolidWorks 2015. Dassault Systemes SolidWorks Corp.

(5) DDBST-GmbH http://ddbonline.ddbst.com/AntoineCalculation/AntoineCalculationCGI.exe?component=Tetrahydrofuran (accessed Feb 25, 2016).

(6) Yokoyama, H. Diffusion of Block Copolymers. *Mater. Sci. Eng. R Reports* **2006**, *53* (5–6), 199–248.

(7) Landry, M. R.; Gu, Q.; Yu, H. Probe Molecule Diffusion in Polymer Solutions. *Macromolecules* **1988**, *21* (4), 1158–1165.

(8) Matsen, M. W.; Bates, F. S. Unifying Weak- and Strong-Segregation Block Copolymer Theories. *Macromolecules* **1996**, *29* (4), 1091–1098.

(9) Lodge, T. P.; Hanley, K. J.; Pudil, B.; Alahapperuma, V. Phase Behavior of Block Copolymers in a Neutral Solvent. *Macromolecules* **2003**, *36* (3), 816–822.

(10) Flory, P. *Principles in Polymer Chemistry*; Ithaca: Cornell University Press, 1978.

(11) Deshpande, D. D.; Patterson, D.; Schreiber, H. P.; Su, C. S. Thermodynamic Interactions in Polymer Systems by Gas-Liquid Chromatography. IV. Interactions between Components in a Mixed Stationary Phase. *Macromolecules* **1974**, *7* (4), 530–535.

(12) Holman, J. P. *Heat Transfer 10th Ed*; Mc-Graw-Hill Companies Inc, New York, NY, 2010.